A peer-reviewed version of this preprint was published in PeerJ on 16 October 2018.

View the peer-reviewed version (peerj.com/articles/5766), which is the preferred citable publication unless you specifically need to cite this preprint.

Villafañe PG, Corbí H, Cónsole-Gonella C, Ruiz-Sánchez FJ, Soria JM. 2018. The Messinian stromatolites of the Sierra del Colmenar (Western Mediterranean): facies characterization and sedimentological interpretation. PeerJ 6:e5766 https://doi.org/10.7717/peerj.5766

The Messinian stromatolites of the Sierra del Colmenar (Western Mediterranean): facies characterization and sedimentological interpretation

Patricio Guillermo Villafañe [Corresp., 1], **Hugo Corbí** [2], **Carlos Cónsole-Gonella** [1], **Francisco Javier Ruiz-Sánchez** [3]

[1] Instituto Superior de Correlación Geológica (INSUGEO), Universidad Nacional de Tucumán-CONICET, Tucumán, Argentina

[2] Department of Earth Sciences and the Environment, Universidad de Alicante, Alicante, Spain

[3] Department of Botany and Geology, Universidad de Valencia, Valencia, Spain

Corresponding Author: Patricio Guillermo Villafañe
Email address: pgvillafane@csnat.unt.edu.ar

The Messinian stromatolites belonging to the Terminal Carbonate Complex unit, from the northern sector of the Bajo Segura Basin (CAM section, Sierra del Colmenar, SE Spain) have been studied. To understand the direct relationship between the morphologies of the stromatolites and their deposition context in order to reconstruct the environmental conditions for their growth, a detailed study of their architecture, external morphology and internal morphology was carried out (macrofabric and microfabric). The stromatolites are made up of domic bodies laterally linked to each other, generating a macrostructure (bioherms) with lateral continuity. This stromatolitic macrostructure presents variations in its internal morphology, giving rise to seven subfacies product of the environmental changes experienced during the growth of the microbial bushes. The stromatolites are arranged parallel of coastline acting as paleogeographic barriers to reduce the physical stress of the environment. Although in general lines suggests a coastal environment, restricted and shallow for the formation of the whole level, the variation in internal morphology is evidence of minor changes in the physical environment.

The Messinian stromatolites of the Sierra del Colmenar (Western Mediterranean): facies characterization and sedimentological interpretation.

Patricio Guillermo Villafañe[1]; Hugo Corbí[2]; Carlos Cónsole-Gonella[1]; Francisco Javier Ruiz-Sánchez[3].

1. Instituto Superior de Correlación Geológica (INSUGEO), Universidad Nacional de Tucumán-CONICET, Tucumán, Argentina.
2. Department of Earth Sciences and the Environment, University of Alicante, Alicante, Spain.
3. Department of Botany and Geology, Universitat de València, Valencia, Spain.

Corresponding author:
Patricio Guillermo Villafañe
e-mail address: pgvillafan@gmail.com

Abstract

The Messinian stromatolites belonging to the Terminal Carbonate Complex unit, from the northern sector of the Bajo Segura Basin (CAM section, Sierra del Colmenar, SE Spain) have been studied. To understand the direct relationship between the morphologies of the stromatolites and their deposition context in order to reconstruct the environmental conditions for their growth, a detailed study of their architecture, external morphology and internal morphology was carried out (macrofabric and microfabric).

The stromatolites are made up of domic bodies laterally linked to each other, generating a macrostructure (bioherms) with lateral continuity. This stromatolitic macrostructure presents variations in its internal morphology, giving rise to seven subfacies product of the environmental changes experienced during the growth of the microbial bushes.

The stromatolites are arranged parallel of coastline acting as paleogeographic barriers to reduce the physical stress of the environment. Although in general lines suggests a coastal environment, restricted and shallow for the formation of the whole level, the variation in internal morphology is evidence of minor changes in the physical environment.

Key-words. Stromatolites, Messinian Salinity Crisis, Bajo Segura basin, Terminal Carbonate Complex, Carbonate sedimentology, Neogene, western Mediterranean

Introduction. In the Bajo Segura basin, a western Mediterranean basin where the different phases (pre-, syn- and post-) of the Messinian Salinity Crisis is represented (Corbí et al., 2016; Corbí & Soria, 2016; Corbí, 2017), where Messinian stromatolites are present in several areas. Stromatolites were first recorded here by Esteban et al. (1978), who reported biohermic stromatolites with hemispherical morphologies from the Messinian age in the area outside Santa Pola. Feldmann (1995) and Feldmann & McKenzie (1997) conducted highly descriptive studies

in the northern section of the Bajo Segura Basin, defining five different types of stromatolitic structures in Messinian deposits in the Santa Pola sector. Later, Soria et al. (2005, 2008) reported the presence of stromatolites in the northern section of the Bajo Segura Basin, in the Messinian II Unit belonging to the Terminal Carbonate Complex (Calvet, 1996), locating them stratigraphically beneath the end-Messinian unconformity. Also, stromatolites have also been reported from the southern sector of the basin, and interpreted as indicators of sudden emersion and subsequent sub-aerial exposure (Corbí, 2010; Corbí et al., 2016).

The stromatolites studied in this paper outcrop at the CAM sequence (named after a nearby former venue of the banking company *Caja de Ahorros del Mediterraneo* [CAM].) They were discovered by a research group from the University of Alicante in the late 1990s. Located outside the city of Alicante, geologically they correspond to the northern sector of the Bajo Segura basin, and their stratigraphic sequence belongs, in the terminology of Calvet et al. (1996) to the Terminal Carbonate Complex (Upper Miocene, Messinian). The aim of the current study is to understand the direct relationship between these stromatolites and their sedimentary environment. For this purpose, the stromatolithic outcrop facies in this sequence will be defined based on the evaluation of the texture, external morphology and variation of the internal structure.

Geological context. The Bajo Segura basin is located at the eastern end of the Betic Cordillera, in southeastern Spain. With a surface area of 3000 Km^2, it is located in the middle of Alicante Province, except for a small sector in the west of the basin which is included in Murcia Province (Corbí, 2010) (Fig. 1). In this basin, two tectonically and palaeogeographically clearly defined sectors can be distinguished in the Bajo Segura basin – North and South – in which the sedimentary record begins in the Tortonian and continues to the Quaternary. This basin presents one of the most complete Miocene and Pliocene records of the Mediterranean margins, showing an exceptional record of the different sedimentological and palaeoenvironmental phases of the Messinian Salinity Crisis (Soria et al., 2008; Caracuel et al., 2011; Soria et al., 2014; Corbí & Soria, 2016; Corbí et al., 2016; 2018; Corbí, 2017). In the northern sector, where our study is focused, the Messinian and Pliocene units present facies associations typical of shallow marine and continental environments; while in the southern sectors, the Messinian and Pliocene units present facies associations corresponding to deeper marine environments (Viseras et al., 2004).

Sequential-stratigraphic analysis has enabled the identification of units bounded by unconformities, or depositional sequences, as follows (from bottom to top): a) The sedimentation sequence in the basin begins during the Tortonian with Synthem T-I, characterized by the predominance of marl facies with large amounts of planktonic organisms; b) Synthem T-II, of Tortonian age, is marked by the intra-Tortonian unconformity and is composed of lithology ranging from fossil-rich marls to conglomerates with sandy matrix (Tent-Manclús, 2003); c) Synthem T-MII is separated by the late-Tortonian unconformity, where the shallow marine conditions that reigned at the end of the Synthem T-II sedimentation are replaced by continental environments in the west and open marine environments in the east (Soria et al., 2001; Tent-

Manclús, 2003); d) Synthem M-II is separated by the intra-Messinian Synthem T-MI unconformity (Soria et al., 2005; Soria et al., 2008). It has been assigned to an upper Turolian – Messinian age (Calvet et al., 1996) and is composed of a lithological variety corresponding to a marine environment of variable depth (Soria et al., 2005); and e) Synthem P, of Pliocene age, is separated from the previous synthem by the late Messinian unconformity and presents marine paleoenvironmental conditions which are subsequent to the desiccation of the Mediterranean (Soria et al., 2005).

The stromatolites analysed in this paper are included in Synthem MII, which is separated from Synthem T-MI by the intra-Messinian unconformity and bounded at the top by the end-Messinian unconformity (Soria et al., 2005; Soria et al., 2008). In the northern sector of the basin, Synthem MII consists of five depositional systems: a) MIIa: red lutites with alternating with sandstones and conglomerates, interpreted as a deposit of distal alluvial fans with a well-drained floodplain; b) MIIb: predominantly limestone and marly limestones with gastropod fossils and root bioturbations, interspersed with layers of red clays and dark marls with rodent fossils. These facies association suggest a lacustrine or pallustrial environment without marine influence; c) MIIc: lutites alternating with marl-limestones with rodent fossils and large channels filled with marls and sands. Interpreted as a flood lagoon in a high-energy fluvial valley; d) MIId: predominantly red and grey marls alternating with massive micritic limestones and channels filled with gravels and sands. Interpreted as a coastal lagoon environment interdigitated to the east with beach deposits (MIIe system); and e) MIIe: found only in the Eastern part of the North Sector, it presents three different facies associations: calcareous marls with bivalves, stromatolitic limestones forming domes over one meter high and oolitic calcarenites with wave ripples. Overall, the system represents several coastal sub-environments from the shoreface to the backshore and was named Terminal Carbonate Complex (Calvet et al., 1996).

Materials and Methods. The CAM section, located a few kilometres west of the city of Alicante (Fig. 1), was selected for analysis of recorded stromatolitic facies. A stratigraphic section was logged, emphasizing stromatolitic facies, and at the same time, material was collected by systematic sampling. Samples were used to prepare thin sections in the Petrology Laboratory at the University of Alicante (Spain) and polished sections in the Industrial Rock Laboratory 1 at the Department of Geology of the University of Valencia (Spain).

Stratigraphic and sedimentological analysis of the sequence followed the methodology proposed by Mercedes-Martin et al. (2014). In addition to facies analysis, was included identification in the field of bounding or stratigraphic surfaces, which may have regional significance.

The study was performed in two stages. In the first stage, external architecture and morphology were analysed based on field and laboratory data, including dimensions and spatial distribution of outcrop structures, general external appearance, colour, types of contacts and thicknesses. Descriptions were based on the proposals of Clarke & Teichert (1946), Logan (1961), Aitken (1967) and Gebelein (1969); supplemented with descriptive terminology from more

contemporary authors such as Davaud et al. (1994), Nehza & Woo (2006), Jahnert & Collins (2011, 2012), Cooper et al. (2013), Perissinotto et al. (2014) and Sousaari et al. (2016). In the second stage, internal morphology was analysed according to macrofabric/general internal structure and microfabric.

For macrofabric, subfacies were distinguished in the field according to textural and lithological variations. The study continued in the laboratory, using hand samples and polished sections to determine internal structures, lamination types, geometrical variations, textural features, presence of clastic material, etc. in each subfacies. The description of macrofabric was based on the classification proposed by Logan et al. (1964) and supplemented with descriptive criteria proposed by Malan (1964), Aitken (1967), Hoffman (1973), Monty (1977), Schneider (1977), Awramik & Vanyo (1986), Acosta et al. (1988), Cohen et al. (1997), Shapiro & Awramik (2000) and Suarez-Gonzales et al. (2014).

Microfabric was analyzed in the laboratory using thin sections to define parameters involved in stromatolite microstructure: lamination types, stacking, lateral and vertical continuity of lamination, growth dynamics, hiatuses, etc.

Stromatolite lamination was analyzed following the concepts proposed by Sarjeant (1975), Scholle (1978), Monty (1977) and Suarez-Gonzales et al. (2014), by describing factors such as composition, lateral continuity, thicknesses, geometrical arrangement, etc. Study of erosional structures was based on the criteria of Schneider (1977), Scholle (1978) and Cevallos-Ferrix & Werber (1980). Porosity was analyzed according to the classification proposed by Choquette & Pray (1970) and the descriptive concepts of Alonso et al. (1987).

Results.

Description of the stratigraphical section. Stratigraphically, in the CAM sequence record the synthems MII and P of Soria et al. (2005; 2008) and Corbí & Soria (2016), ranging from late Messinian to Lower Pliocene. The section includes the stromatolites from Terminal Carbonate Complex of Calvet et al. (1996), which are recorded in the Synthem MII of the later authors.

Lithologically, the studied sequence is largely composed of alternating tabular strata of calcareous marls, calcarenites and limestones; sloping approximately 15º to SE (Fig. 2). From the bottom of the profile up to approximately 2.5 meters, there are predominantly calcareous sandstone lithologies alternating with layers of lutites. From 2.5 meters up, there are micritic limestone strata; and it is in one of these strata, between 3.5 and 5.0 meters, that the stromatolitic structures are found which are studied in detail in this paper. Above these is a layer of calcarenite, which follows the stromatolite morphology.

At 5 meters there is an erosive surface in the profile, with predominantly subhorizontal – though irregular – morphology, which affects both the stromatolitic domes and the calcarenite layer (Fig. 3). This erosive surface, known as the end-Messinian unconformity, was studied in detail by Soria et al. (2008) and Corbí (2010). It is of great regional and stratigraphic importance because it separates MII units of the upper Messinian from the P units of the lower Pliocene. The erosive event is related to the Messinian Salinity Crisis record on the margins of the

Mediterranean, generated by subaereal exposure at the edges of the basin (Soria et al., 2005, 2008). Above the end-Messinian unconformity, the sequence concludes with a tabular stratum of calcarenite with bioperforations at the base.

Architecture and external morphology of the Stromatolites. Stromatolitic structures developed on an irregular substrate of calcareous composition (mudstones) are present throughout the entire horizontal continuity of the layer between 3,50 and 5,00 meters. They are described as "domical" bodies up to 2.00 meters tall and radius 1.50 meters, laterally linked to each other by structures that are semi-parallel to the substrate, called "interdomes", which may be up to 1.00 meter thick and 4.00 meters long. The macrostructure of the stromatolite level consists of concave-convex shapes. The domes are in direct contact with each other in some sectors, and connected by the "interdome" structures in others (Fig. 3). Superficially (external morphology), the stromatolites present morphology which has been described as colloform by other authors in analogous deposits (e.g. Davaud et al., 1994; Nehza & Woo, 2006; Jahnert & Collins, 2011; 2012; Cooper et al., 2013; Perissinotto et al., 2014; Sousaari et al., 2016). The interdome spaces are filled with calcarenite of medium grain and massive texture. It should be noted that not all domes are fully preserved, as some of them were cut by the end-Messinian discontinuity, as shown in figure 3.

Internal stromatolite morphology: characterization of subfacies. The stromatolite sequence shows seven textural and structural variations along their vertical development, which could be defined as subfacies (Fig. 4). These subfacies are present throughout the entire macrostructure, in both domical and interdome areas, generating an internal structure which Logan et al. (1964) called LLH (laterally linked hemispheroids). In the current study, the zones where domes are in contact with each other are type LLH-C (close lateral linkage hemispheroids), while the zones where the domes are connected by "interdome" structures are type LLH-V (spaced lateral linkage hemispheroids) (Logan et al., 1964). For description of their macrofabric and microfabric, the subfacies are numbered from one to seven, following stromatolite growth direction, being (1) the oldest and seven (7) the newest. In addition, any lateral variation is mentioned for regions defined as large domes or interdomes.

Subfacies 1: It is not very thick in the interdome area, but becomes vaulted and up to 0,60 meters thick within domes, forming their nuclei. As we ascend in these subfacies, following the direction of growth, the porosity of Vuggy (sensu Choquette & Pray, 1970) increases; and signs of lamination begin to appear, although it is too diffuse to be classified.

Microfabric analysis shows that the interdome sector is composed entirely of micritic mud with massive texture and no pattern of arrangement (Fig. 5A). Porosity is 50% of the surface of the section, with non-fabric-selective vuggy pores (*sensu* Choquette & Pray, 1970) with diameters ranging from 50µm to 400µm.

In the upper part of the dome sector there are alternating micritic laminae, which repeat cyclically giving rise to a "repetitive" type microfabric (*sensu* Monty, 1977) (Fig. 5B). Laminae

are 200µm to 500µm thick, continuous and slightly sinuous, with boundaries having diffuse texture (*sensu* Sarjeant, 1975). Porosity in this sector is only 5%, with both vuggy (non-fabric-selective) and fenestral (fabric-selective) types (*sensu* Choquette & Pray, 1970).

Subfacies 2: The macrofabric is characterized by clearly alternating calcareous laminae, 10 cm to 15 cm thick, which are continuous throughout the entire horizontal development of stromatolites. Lamination is densely packed, with continuous, straight, not very sinuous laminae with diffuse boundaries. Logan et al. (1964) calls this type of structure LLH-V.

In the interdome area there are alternating micritic laminae (more than 65%) and intramicritic laminae (less than 35%), which repeat cyclically, giving rise to a repetitive microfabric type (*sensu* Monty, 1977) (Fig. 5C).

The thickest laminae (up to 1.5mm) are those of intramicritic composition (Folk, 1959), which are composed of micritic intraclasts and bioclasts immersed in a micritic matrix. Micrite layers are 50µm to 100µm thick.

Intraclasts are composed of lithified micritic sediment (100µm and 400µm) and grouped in small pockets up to 700µm in diameter, surrounded by micritic mud. Bioclasts may measure up to 200µm and are randomly scattered throughout the intramicritic lamination. Porosity is only 35%, and includes vuggy, moldic (non-fabric-selective) and "fenestral" (fabric-selective) types (*sensu* Choquette & Pray, 1970).

Microfabric in the dome area was found to be composed of repetitive alternation (*sensu* Monty, 1977) of micritic laminae (Fig. 5D). Laminae are less than 300µm thick, laterally continuous, slightly wavy and have boundaries with diffuse texture (*sensu* Sarjeant, 1975), so there is transitionality between one lamina and the next.

Porosity is 10%, with non-fabric-selective vuggy porosity and cavities; as well as fabric-selective fenestral type porosity (*sensu* Choquette & Pray, 1970).

Subfacies 3: Subfacies 3 it is characterized by the absence of lamination. Its thickness is virtually constant, ranging from 0,15 to 0,25 meters.

There are sectors with lithified micritic sediment intraclasts up to 300 µm across, sometimes grouped in small pockets up to 600µm across and other times scattered randomly throughout the micritic matrix. Porosity is not more than 10% of the surface of the section, with vuggy non-fabric-selective porosity being the most plentiful (*sensu* Choquette & Pray, 1970). It is worth noting the presence of sub-rounded, concentric ooliths with micritic nuclei, up to 400 µm across submerged randomly in the micritic matrix (Fig. 5F).

Subfacies 4: In the macrofabric there is clear alternation of continuous, densely packed calcareous laminae which become thinner from bottom (1.20mm) to top (0.5mm), generating a structure called LLH-V by Logan et al. (1964). The thickness of this subfacies is practically constant throughout its horizontal development, ranging from 0,1 to 0,2 meters.

In both the interdome and the dome areas, stromatolite microfabric is characterized by the presence of alternating micritic laminae which repeat in similar patterns (color, thicknesses and

laminae boundaries) giving rise to a repetitive type microfabric (*sensu* Monty,1977) (Fig. 6A y 6B). Laminae are up to 200µm thick, wavy, poor in intraclasts and have diffuse boundaries (*sensu* Sarjeant, 1975), so there is transitionally from one lamina to another (Fig. 6B). Porosity is 2% to 4%, with non-fabric-selective vuggy type morphology (*sensu* Choquette & Pray, 1970).

Subfacies 5: It is the thickest, being 1 meter thick in the zone with large domes and up to 0,8 meters thick in the interdome zone. Its macrofabric is characterized by alternating calcareous laminae up to approximately 1mm thick, continuous but with irregular morphology, with waves having low amplitude and high frequency, giving rise to what Logan et al. (1964) call LLH-C.

In the interdome area, the microfabric is characterized by alternating micritic laminae, which repeat over a continuous growth cycle, giving rise to a repetitive type microfabric (*sensu* Monty, 1977). Laminae thickness varies from less than 100µm to 1mm; laminae are wavy with diffuse texture boundaries (*sensu* Sarjeant, 1975), so there is transitionally in the passage from one lamina to another (Fig. 6C). An average of fields suggests 20% porosity, with pores up to 500µm and non-fabric-selective vuggy porosity (*sensu* Choquette & Pray, 1970).

The dome sector microfabric is composed of alternating micritic laminae (60%) and intramicritic laminae (40%). However, the lamination has no defined order, so it is a simple alternate type sequence (*sensu* Monty, 1977) (Fig. 6D). Although micritic laminae are more plentiful, they are thinner (100µm to 300µm), while intramicritic laminae may be up to 1 mm thick. Lamination is continuous. Laminae are straight but with well-marked waves and diffuse boundaries (*sensu* Sarjeant, 1975), so there is transitionally from one lamina to another. Intraclasts present in the intramicrites are smaller than 300µm, micritic and subrounded.

Porosity accounts for 15% of the total surface of the section and includes both non-fabric-selective vuggy porosity and fabric-selective fenestral and mold porosity (*sensu* Choquette & Pray, 1970).

Subfacies 6: Is defined by a series of columnar structures of constant basal radius composed of alternating laterally interrupted calcareous laminae, giving rise to an SH type structure (vertically stacked hemispheroids) type C (constant basal radius) (Logan et al., 1964). This subfacies shows continuity throughout the horizontal development of the stromatolites, and constant thickness of 0,25 to 0,30 meters.

There are no bifurcations over their vertical development of the columns, although there are surfaces indicating interruption over their growth (hiatuses) and signs of repair among columns. The cavities formed by the interruption of lateral continuity of lamination are up to 0,5 cm thick and filled with mudstone with massive texture.

The microfabric does not vary between domes and interdomes. Laminae are composed of micrite and repeat in a continuous cycle, with similar patterns (color, thickness and boundaries of laminae), giving rise to a “repetitive” type microfabric (*sensu* Monty, 1977). Lamination is wavy and laterally interrupted, creating cavities. Most laminae have boundaries with diffuse texture (*sensu* Sarjeant, 1975), so there is transitionality from one lamina to another (Fig. 7A y 7B)

Estimated porosity is 20% to 25% with pores of both non-fabric-selective with vuggy and channel porosity (by fracture), and fabric-selective with fenestral and moldic porosity (*sensu* Choquette & Pray, 1970).

Subfacies 7: Is 0,15 to 0,20 meters thick and is the subfacies at which stromatolite vertical development ends. It is defined by a series of columnar constructions composed of alternating laterally interrupted calcareous laminae. Logan et al. (1964) calls this type of columnar structure SH type V (variable basal radius).

The columnar structures are 0.5cm to 2cm in diameter, with variable basal radius. There are no bifurcations over the vertical development of the columns, but there are interruption surfaces (hiatuses) over their growth. In contrast to the columnar structures in subfacies 6, these are more rounded and there is no sign of repair between mats. The cavities formed by the interruption of the lateral continuity in lamination are up to 1cm thick and filled with micrite with no clearly defined pattern of arrangement.

It should be noted that the dome zone in this subfacies is eroded by the late-Messinian unconformity.

The microfabric in this subfacies is characterized by alternate micritic laminae, creating a repetitive type microfabric (*sensu* Monty, 1977). The laminae are 100µm to 1mm thick, wavy and concave upward. Most laminae have boundaries with diffuse texture (*sensu* Sarjeant, 1975), so there is transitionality from one lamina to another (Fig. 7C y D). There are bifurcations along some laminae.

Porosity is 10% with both non-fabric-selective fabric vuggy type morphology and fabric-selective with fenestral porosity (*sensu* Choquette & Pray, 1970). Pore diameters are less than 500µm.

Discussion.

Facies interpretation and depositional model. The stromatolitic ecosystems of Sierra del Colmenar (CAM section, SE Spain) are wide ranging in areas parallel to the coast, although they are complicated by topographic irregularity, sediment accumulation patterns and water drainage (Golubic, 1985; Bauld, 1986). In the studied sequence, carbonate stromatolites are highly developed both in thickness and in lateral continuity, which Riding (2011) explains as major time intervals during which biological factors prevailed over physical and chemical factors. During those intervals, stromatolite growth was enabled by a regular and especially uniform supply of sediment at surfaces colonized by layers of microbial mucilage (Braga et al., 1995) in an environment with relatively low hydrodynamic energy and high salinity (Feldmann & McKenzie, 1997). However, the diversity of internal morphology present in the development of the stromatolites suggests that environmental conditions during their growth underwent variations (Logan, 1961; Logan et al., 1964; Monty, 1977; Awramik & Vanyo, 1986; Andres & Reid, 2006; Allwood et al., 2009).

The direct relationship between stromatolite morphology and its depositional context enables paleoenvironmental models to be developed (Black, 1933; Young, 1935; Clarke & Teichert,

1946; Ginsburg, 1955; Rezak, 1957; Reid et al., 2000; among others). This is why some authors like Riding et al. (1991) and Calvet et al. (1996) suggest that restricted paleoenvironmental conditions and high salinity would be the cause of the presence of stromatolitic structures throughout the Terminal Carbonate Complex.

External morphology. The external morphology of the stromatolites in the CAM sequence is Domical Colloform (Jahrnet & Collins, 2012), suggesting that the final stromatolite growth stage (represented by subfacies 7) took place in a protected environment at a depth of less than 2 m (Davaud et al., 1994; Nehza & Woo, 2006; Jahnert & Collins, 2011; Cooper et al., 2013; Perissinotto et al., 2014; Sousaari et al., 2016).

Stromatolite architecture and morphology is mainly affected by environmental factors, in particular water depth, wave energy, pre-existing substrate, sediment influx and lithification (Grotzinger & Knoll, 1999; Kah & Bartley, 2004; Kah et al., 2006; Andres & Reid, 2006; Allwood et al., 2009). The macrostructure architecture can be attributed to the growth of microbial mats that "follow" the irregularities of the underlying substrate in shallow waters (Logan et al, 1964; Cohen et al., 1997; Allwood et al., 2009), added to continuous expansion of their lateral growth (Logan et al., 1964). But the most parsimonious hypothesis is that the "domical" shapes would be the outcome of stromatolite response to the need to minimize the force of water acting upon them (*sensu* Gebelein, 1969), while the "interdome" shapes would serve as large discharge areas (Ceballos-Ferris & Weber, 1980). Some authors like Feldmann & McKenzie (1997) and Mercedes-Martin et al. (2014), suggest that stromatolitic macrostructures of this size acted as a palaeogeographic barrier, reducing physical stress and erosion, and fostering restricted conditions in response to falling sea level and the increase in the hydrodynamic energy of the environment.

The end of stromatolitic level growth is attributed to a change in environmental conditions as a result of shallowing of the water body, generating a prevalence of physical and chemical factors over biological factors (Schubert & Bottjer, 1992; Mercedes-Martin et al., 2014).

Finally, the end-Messinian discontinuity represents a baseline level on a regional scale (Soria et al., 2008). It represents three hiatuses in the stratigraphic sequence: (1) an erosional hiatus associated to the drop in sea level as a result of the Salinity Crisis, in which stromatolitic domes and interdome filling were shaped; (2) a non-depositional hiatus comprising the time lapsed until the rising sea level reached the erosion surface developed, and (3) a final erosional hiatus as a result of the Pliocene transgression, when coastal erosion once again eliminated part of the stromatolitic unit and its filling. Equivalent hiatus and progression of paleoceanographic events have been described by Caracuel et al. (2004) in the northern border of the Bajo Segura basin, where our study is focused.

Internal morphology. In the CAM sequence, stromatolites, have LLH type macrostructure, which is type C in some sectors and type V in others. This kind of macrostructure is observed in current shallow marine environments near the coastline, where domes are shallowly submerged

and receive good light intensity. They also indicate low-energy hydrodynamic conditions enabling mats to develop with high lateral continuity (Castro & Ruiz-Ortiz, 1991; Reid et al., 2000) (Fig. 8).

Stromatolite internal morphology is controlled by various parameters. Macrostructure and macrofabric are mainly controlled by environmental factors such as light, depth, substrate type, temperature and water turbidity, whereas microfabric is mainly controlled by chemical and biological factors (Riding, 2011). Thus, the variation in internal morphology over vertical growth provides direct evidence of changes in the environment (Logan, 1961; Logan et al., 1964; Braga et al., 1995).

Subfacies 1 suggests a reduction in hydrodynamic energy from bottom to top. This is represented by a basal sector lacking stromatolitic lamination and suggesting medium to high hydrodynamic conditions (Gebelein, 1969; Acosta et al., 1988; Castro & Ruiz-Ortiz, 1991; Reid et al., 2000), while upwards, we begin to see fine, continuous lamination, indicating a reduction in environmental hydrodynamic conditions (Logan et al., 1964; Acosta et al., 1988).

On the other hand, stromatolitic lamination is greater in the dome zone than the interdome zone. This suggests that although they were formed contemporaneously, the hydrodynamic energy was higher in the interdome sector than in the dome sector, with the interdomes being interpreted as water discharge and runoff channels (Ceballos-Ferris & Weber, 1980; Mercedes-Martin et al., 2014).

In subfacies 2, the LLH-V type macrostructure suggests an environment with constant humidity and low hydrodynamic energy, which enabled stromatolitic mats to achieve horizontal continuity (Logan et al., 1964) and the presence of "repetitive" lamination (*sensu* Monty, 1977) because cyclical variations in environmental factors with favourable conditions throughout the development of this subfacies (Riding, 2008; Decho, 2000; Riding, 2011). In the dome zone, lamination is of micritic composition, indicating that the domes were exposed to lower hydrodynamic energy (Monty, 1977; Reid et al.; 2000; Suarez–Gonzales et al., 2014) than the interdome zone, where micritic and intramicritic laminae alternate, indicating time periods with occurrence of temporary increases in the hydrodynamic energy of the environment (Scholle, 1978; Mercedes-Martin et al., 2014).

Regard to subfacies 3, the absence of lamination can be caused by time intervals where the physical, chemical or biological conditions were not appropriate for mat growth (Riding, 2008). The presence of lithified micrite intraclasts grouped in pockets is a result of transportation of autochthonous or para-autochthonous sediment during intervals of greater energy (Acosta et al., 1988; Castro & Ruiz-Ortiz, 1991), while the presence of concentric oolites suggests hydrodynamic conditions with high energy in shallow environments (Rohrlich, 1974; Calvet el al., 1996). However, it should be noted that horizontal continuity and constant thickness of this subfacies throughout the entire stromatolite surface suggest biological influence in its generation.

In subfacies 4, the LLH-V macrofabric indicates conditions of constant humidity, low hydrodynamic energy and good lighting, suggesting a shallow subtidal to low intertidal environment (Logan et al., 1964; Jahnert & Collins, 2012), where microbial activity increases

notably, enabling stabilization of laminae (Reid et al., 2000; Suarez-Gonzales et al., 2014). The microfabric in this subfacies presents no change between dome and interdome zones, while the presence of laminae that are thicker at the base suggests greater sedimentary input as a result of a stage of greater hydrodynamic energy in this sector of the subfacies (Reid et al., 2000). However, the continuity in the lamination cycle and the diffuse boundaries of the laminae suggest uninterrupted growth over the sedimentary accretion along with a gradual increase in depth (Monty, 1977).

For the subfacies 5, the LLH-C type macrofabric (Logan et al., 1964), according to studies in analogous examples, suggests formation in a subtidal environment with low hydrodynamic energy, enabling microbial mats to develop without lateral interruptions (Riding, 2008; Jahnert & Collins, 2012; Sousaari et al., 2016). The great vertical development of this subfacies is explained for an increase in the depth of the environment, triggering heliotropic growth of microbial mats to ensure better lighting levels (Malan, 1964; Gebelein, 1969; Awramik & Vanyo, 1986; Cohen et al., 1997). It is worth noting that the change from LLH-V (subfacies 4) to LLH-C type morphology may be explained as a response to the need to increase the specific surface of laminae in order to compensate the loss of lighting as a result of increasing environmental depth during flooding episodes (Malan, 1964; Gebelein, 1969; Awramik & Vanyo, 1986; Cohen et al., 1997).

In the interdome sector of subfacies 5, microfabric consists of micritic lamina in “repetitive” type sequences (*sensu* Monty, 1977), suggesting an environment with low hydrodynamic energy in which microbial activity stabilizes the crystals precipitated *in-situ* during a hiatus in accretion (Monty, 1977; Reid et al.; 2000; Suarez–Gonzales et al., 2014). On the other hand, in the domes sector of this subfacies, micritic laminae alternate with intramicritic laminae, forming a “simple alternate” sequence (*sensu* Monty, 1977). Ginsburg (1955) suggest that the fact that intramicritic laminae are present only in the dome sector may be the result of flooding episodes, during which there is more active binding of sediment in the parts with greater relief and therefore lamination with larger grain size.

Subfacies 6 has SH-C type internal structure (Logan et al., 1964), suggesting a shallow, low intertidal environment, with medium to low hydrodynamic energy, where waves are the main mechanical factor. Columnar structures are the result of differential erosive effect during discharge and runoff of water along “channels”, truncating the microbial mats *in vivo* and preventing lateral development of lamination (Schneider, 1977; Cevallos-Ferrix & Werber, 1980; Acosta et al., 1988; Shapiro & Awramik, 2000). The transition from LLH morphology in subfacies 5 to SH morphology in subfacies 6 suggests an increase in environmental hydrodynamic energy (cf. Acosta et al., 1988).

Subfacies 6 is composed of micrite laminae in a “repetitive” sequence (*sensu* Monty, 1977), both in the “dome” and the “interdome” zones. This suggests that environmental hydrodynamic energy allowed microbial activity to stabilize micritical laminae (Monty, 1977; Reid et al.; 2000; Suarez–Gonzales et al., 2014).

In subfacies 7, macrofabric is type SH-V (Logan et al., 1964), suggesting a shallow environment with low to medium hydrodynamic energy, which, as mentioned above, is the result of the erosive effect during water discharge and runoff through channels, preventing mat growth (Schneider, 1977; Cevallos-Ferrix & Werber, 1980; Acosta et al., 1988; Shapiro & Awramik, 2000). It should be mentioned that the passage of an internal structure of type SH-C (subfacies 6) to one of the SH-V type (subfacies 7) is caused by a continuous loss of the depth of the environment and the increase of hydrodynamic energy (Cevallos-Ferrix & Weber, 1980; Kah & Bartley, 2004; Kah et al., 2006).

Subfacies 7 microfabric consists of micritic laminae in "repetitive" sequences (*sensu* Monty, 1977) suggesting prevalence of biological factors in the environment. However, the absence of signs of repair between mats suggests higher hydrodynamic energy in its formation than in subfacies 6 (Cevallos-Ferrix & Werber, 1980).

It is worth noting that fossil material (microfossils), or evidence of it, is only found in stromatolite basal subfacies, but disappears in the direction of dome growth. Authors such as Mercedes-Martin et al., (2014) explain this as a result of a progressive increase in environmental salinity, possibly associated to high evaporation rates under restricted arid conditions. On the other hand, although there are several porosity morphologies and fabrics, they do not provide much environmental information. Non-fabric-selective porosity (pockets or vuggy porosity) are a result of diagenetic processes subsequent to stromatolite formation (Choquette & Pray, 1970), whereas fenestral porosity may originate as retraction parallel to lamination as a result of its desiccation (Alonso et al., 1987), or due to gas bubbles formed by rotting organic matter (Sanz-Montero et al., 2005).

Conclusions. The CAM sequence located in the Sierra del Colmenar, presents a highly developed stromatolitic level, both horizontally and vertically, in response to environmental modifications resulting from a progressive drop in sea level. The analysis of facies relationships enable us to infer that the stromatolites were formed in a restricted, subtidal-intertidal to supratidal environment with saturated waters.

The macrostructure of the stromatolitic level consists of domical and interdome forms arranged parallel to the coast and acting as a palaeogeographic barrier, reducing physical stress, channelling the erosive effect of water and favouring restricted conditions. The most parsimonious hypothesis is that the domical shapes were formed as a stromatolite response to minimize the force of the water acting upon them, while the interdome forms would act as large discharge areas.

In general, a similar environment is suggested for the formation of the entire stromatolitic level. However, the variation in internal morphology over vertical stromatolite growth provides evidence of minor changes in the physical environment during the development of each stromatolitic subfacies.

The upper part of subfacies 1 is where stromatolitic lamination is first visible, marking the beginning of a subtidal environment with conditions of constant humidity and low hydrodynamic energy, which is maintained throughout the development of subfacies 2.

Subfacies 3 represents a sudden loss of depth and an increase in hydrodynamic wave energy, expressed in the absence of stromatolitic lamination and the presence of oolites. However, at the transition to subfacies 4, a progressive increase in depth begins, in conditions of low hydrodynamic energy, giving rise to LLH-V lamination cycles. This increase in depth reaches a maximum during subfacies 5, providing more space, great vertical development and a change to LLH-C macrofabric in a subtidal environment.

The transition from subfacies 5 to 6 indicates a gradual decrease in depth, reaching an intertidal wave-dominated environment, resulting in SH-C type internal structure. During the formation of subfacies 7, shallowing continued, generating columnar SH-V type structures in response to the increase in wave action at depths of less than 2 meters.

Continuous shallowing puts an end to stromatolite growth and generates precipitation of calcareous-sedimentary material in interdome spaces. Finally, domes and interdome filling material undergo sub-aerial exposure and are shaped by an erosive process, as represented by the end-Messinian discontinuity.

Acknowledgments. This paper was written in the context of the Paleoenvironmental Changes research group (vigrob-167).

The personnel of the laboratory of petrology of the University of Alicante are thanked for the realization of the polished and thin cuts; and the space provided by the University of Valencia for the study of them.

References.

Acosta P, Garcia Hernandez M, Checa A. 1988. Biohermos de esponjas y estromatolitos en la secuencia transgresiva oxfordiense de la Sierra de Cazorla. Geogaceta, 5: 36-39.

Aitken JD. 1967. Classification and environmental significance of cryptalgal limestones and dolomites. Journaly of Sedimentology and Petrology, 37: 1163-1178.

Allwood AC, Grotzinger JP, Knoll AH, Burch IW, Anderson MS, Coleman ML, Kanik I. 2009. Controls on development and diversity of Early Archean stromatolites. Proceedings of the National Academy of Sciences, 106(24): 9548-9555.

Alonso FJ, Esbert RM, Ordaz J. 1987. Caracterizacion del sistema poroso de calizas y dolomias. Boletin Geologico y Minero, 98: 226-237.

Andres MS, Reid RP. 2006. Growth morphologies of modern marine stromatolites: a case study from Highborne Cay, Bahamas. Sedimentary Geólogy, 185(3): 319-328.

Awramik SM, Vanyo JP. 1986. Heliotropism in modern stromatolites. Science, 231: 1279-1281.

Bauld J. 1986. Benthic microbial communities of Australian saline lakes. In: De Deckker P, Willams D, eds. *Limnology in Australia.* Springer Netherlands, 95-111.

Black M. 1933. The algal sediments of Andros Island, Bahamas. Philosophical Transactions of the Royal. Society of London, 122: 165-192.

Braga JC, Martin JM, Riding R. 1995. Controls on microbial dome fabric development along a carbonate-siliciclastic shelf-basin transect, Miocene, SE Spain. Palaios, 10: 347-361.

Calvet F, Zamarreno I, Valles D. 1996. Late Miocene reefs of the Alicante–Elche Basin, southeast Spain. In: Franseen E, Esteban M, Ward W, Rouchy JM, eds. *Models for Carbonate Stratigraphy from Miocene Reef Complexes of the Mediterranean regions, Concepts in Sedimentology and Paleontology.* Series, 5: 177–190.

Caracuel JE, Soria JM, Yebenes A. 2004. Early Pliocene transgressive coastal lags (Bajo Segura Basin, Spain): a marker of the flooding after the Messinian salinity crisis. Sedimentari Geology, 169: 121– 128.

Caracuel JE, Corbí H, Giannetti A, Monaco P, Soria JM, Tent-Manclús JE, Yébenes A. 2011. Paleoenvironmental changes during the late Miocene (Messinian)-Pliocene transition: sedimentological and ichnological evidence. Palaios, 26: 754–766.

Castro JM, Ruiz Ortiz PA. 1991. Nivel condensado con estromatolitos pelágicos en el Cretácico de la Sierra de Estepa (Subbetico Externo, prov. Sevilla). Revista de la Sociedad Geológica de España, 4: 305-319.

Cevallos Ferriz S, Werber R. 1980. Arquitectura, estructura y ambiente de deposito de algunos estromatolitos del Precambrico sedimentario de Caborca, Sonora. Revista Mexicana de Ciencias Geologicas, 4(2): 97-103.

Choquette PW, Pray LC. 1970. Geologic nomenclature and classification of porosity in sedimentary carbonates. The American Association of Petroleum Geologists Bulletin, 54(2): 207-250.

Clarke E, Teichert C. 1946. Algal structures in a West Australian salt lake. American Journal of Science, 224(4): 271-276.

Cohen AS, Talbot MR, Awramik SM, Dettman DL, Abell P. 1997. Lake level and paleoenvironmental history of Lake Tanganyika, Africa, as inferred from late Holocene and modern stromatolites. Geological Society of American Bulletin, 109(4): 444-460.

Cooper JA, Smith AM, Arnscheidt J. 2013. Contemporary stromatolite formation in high intertidal rock pools, Giant's Causeway, Northern Ireland: preliminary observations. Journal of Coastal Research, 65(2): 1675-1680.

Corbí H. 2010. Los foraminíferos de la Cuenca neogena del Bajo Segura (sureste de Espana): bioestratigrafía y cambios paleoambientales en relación con la Crisis de salinidad del Mediterraneo. D. Phil. Thesis, Universidad de Alicante.

Corbí H. 2017. El registro sedimentario de la Cuenca del Bajo Segura (SE España) a través del análisis de correspondencia: implicaciones paleoambientales. Estudios Geológicos, 73(2): 071.

Corbí H, Jesús MS. 2016. Late Miocene–early Pliocene planktonic foraminifer event-stratigraphy of the Bajo Segura basin: A complete record of the western Mediterranean. Marine and Petroleum Geology, 77(2016): 1010-1027.

559 Corbí H, Soria JM, Lancis C, Giannetti A, Tent-Manclús J, Dinares-Turell J. 2016.
560 Sedimentological and paleoenvironmental scenario before, during, and after the Messinian
561 Salinity Crisis: The San Miguel de Salinas composite section (western Mediterranean).
562 Marine Geology, 379: 246–266.
563 Corbí H, Fierro I, Aberasturi A, Ferris EJS. 2018. Potential use of a significant scientific geosite:
564 The Messinian coral reef of Santa Pola (SE Spain). Geoheritage, 1-15.
565 Davaud E, Strasser A, Jedoui Y. 1994. Stromatolite and serpulid bioherms in a Holocene
566 restricted lagoon (Sabkha El Melah, southeastern Tunisia). Phanerozoic Stromatolites, 2: 131-
567 151.
568 Decho AW. 2000. Microbial biofilms in intertidal systems: an overview. Continental Shelf
569 Research, 20(10): 1257-1273.
570 Esteban M, Calvet F, Dabrio C, Baron A, Giner J, Pomar L, Salas R, Permanyer A. 1978.
571 Aberrant features ofthe Messinian coral reefs, Spain. Acta Geológica Hispanica XIII, 1: 20-
572 22.
573 Feldmann M. 1995. Controls on stromatolite formation: A comparative study of modern
574 stromatolites from the Bahamas with Messinian examples from southeast Spain. D. Phil.
575 Thesis, Eidgenossische Technische Hochschule.
576 Feldmann M, McKenzie JA. 1997. Messinian stromatolite-thrombolite associations, Santa Pola,
577 SE Spain: an analogue for the Palaeozoic. Sedimentology, 44(5): 893-914.
578 Folk RL. 1959. Practical petrographic classification of limestones. AAPG Bulletin, 43(1): 1-38.
579 Gamonal A, Mansino F, Ruiz Sanchez FJ, Crespo VD, Corbi H, Montoya P. 2018. Sierra del
580 Colmenar 1A, a new late Messinian (Late Miocene) locality in the Bajo Segura basin (SE
581 Espain): Bioestratigraphic and palaeoenvironmental implications. Historical Biology, 30(3):
582 380-391.
583 Gebelein CD. 1969. Distribution, morphology, and accretion rate of recent subtidal algal
584 stromatolites, Bermuda. Journal of Sedimentary Petrology, 39: 49-69.
585 Ginsburg RN. 1955. Recent stromatolitic sedi-ments from South Florida (abs.). Journal of
586 Paleontology, 29: 723.
587 Golubic S. 1985. Microbial mats and modern stromatolites in Shark Bay, Western Australia. In:
588 Caldwell DE, Brierley JA, Brierley CL, eds. *Planetary ecology*. New York: Van Nostrand
589 Reinhold, 3-16.
590 Grozinger JP, Knoll AH. 1999. Stromatolites in Precambrian carbonates: Evolutionary mileposts
591 or environmental dipsticks?. Annual Reviews of Earth and Planetary Sciences, 27: 313–358.
592 Hoffman HJ. 1973. Stromatolites: characteristics and utility. Earth Science Review, 9(4): 339-
593 373.
594 Jahnert RJ, Collins LB. 2011. Significance of subtidal microbial deposits in Shark Bay,
595 Australia. Marine Geology, 286: 106-111.
596 Jahnert RJ, Collins LB. 2012. Characteristics, distribution and morphogenesis of subtidal
597 microbial systems in Shark Bay, Australia. Marine Geology, 306: 115-136.

598 Kah LC, Bartley JK. 2004. Growth dynamics of stromatolite reefs in the Mesoproterozoic Atar
599 Group, Mauritania. Geological Society of America, abstracts with programs Southeast
600 Section, 36: 111.
601 Kah LC, Bartley JK, Frank TD, Lyons TW. 2006. Reconstructing sea-level change from the
602 internal architecture of stromatolite reefs: an example from the Mesoproterozoic Sulky
603 Formation, Dismal Lakes Group, arctic Canada. Canadian Journal of Earth Sciences, 43: 653–
604 669.
605 Logan BW. 1961. Cryptozoon and Associate Stromatolites from the Recent, Shark Bay, Western
606 Australia. The Journal of Geology, 69: 517-533.
607 Logan BW, Rezak R, Ginsburg RN. 1964. Classification and environmental significance of algal
608 stromatolites. The Journal of Geology, 72: 68-83.
609 Malan SP. 1964. Stromatolites and other algal structures at Mufulira, Northern Rhodesia.
610 Economic Geology, 59(3): 397-415.
611 Mercedes-Martin R, Salas R, Arenas C. 2014. Microbial-dominated carbonate platforms during
612 the Ladinian rifting: sequence stratigraphy and evolution of accommodation in a
613 fault-controlled setting (Catalan Coastal Ranges, NE Spain). Basin Research, 26(2): 269-296.
614 Monty C. 1977. Evolving concepts on the nature and ecological significance of stromatolites. In:
615 Flugel E, ed. *Fossil Algae*. Berlin: Springer Heidelberg, 15–35.
616 Nehza O, Woo KS. 2006. The effect of subaerial exposure on the morphology and
617 microstructure of stromatolites in the Cretaceous Sinyangdong Formation, Gyeongsang
618 Supergroup, Korea. Sedimentology, 53(5): 1121-1133.
619 Perissinotto R, Bornman TG, Steyn PP, Miranda NA, Dorrington RA, Matcher GF, Peer N.
620 2014. Tufa stromatolite ecosystems on the South African south coast. South African Journal
621 of Science, 110(9-10): 01-08.
622 Reid RP, Visscher PT, Decho AW, Stolz JF, Bebout BM, Dupraz C, Macintyre IG, Paerl HW,
623 Pinckney JL, Prufert Beboult L, Steepe TF, Des Marais DJ. 2000. The role of microbes in
624 accretion, lamination and early lithification of modern marine stromatolites. Nature, 406:
625 989–992.
626 Rezak R. 1957. Stromatolites of the Belt series in Glacier National Park and vicinity, Montana.
627 United States Geological Survey, 294: 127-154.
628 Riding RE. 2008. Abiogenic, microbial and hybrid authigenic carbonate crusts: components of
629 Precambrian stromatolites. Geologica Croatia, 61: 73-103.
630 Riding RE. 2011. The Nature of Stromatolites: 3,500 Million Years of History and a Century of
631 Research. In: Reitner J, Queric N, Arp G, eds. *Advances in Stromatolite Geobiology*. Berlin:
632 Springer Heidelberg, 131: 29-74.
633 Riding RE, Braga J, Martin JM. 1991. Oolite stromatolites and thrombolites, Miocene, Spain:
634 analogues of Recent giant Bahamian examples. Sedimentary Geology, 71(3-4): 121-127.
635 Rohrlich V. 1974. Microstructure and microchemistry of Iron Ooliths. Mineralium Deposita, 9:
636 133-142.

637 Sanz Montero ME. Rodriguea-Aranda JP, Calvo JP. 2005. Biomineralization in relation with
638 endoevaporitic microbial communities. Miocene lake deposits of the Madrid Basin, Central
639 Spain. Geophysical Research Abstract, 7: 68-74.
640 Sarjeant WA. 1975. Plant trace fossils. In: Frey RW, ed. *The study of trace fossils*, Berlin:
641 Springer Heidelberg, 163-179.
642 Schneider J. 1977. Carbonate construction and decomposition by epilithic and endolithic
643 microorganisms in salt-and freshwater. In: Flugel E, ed. *Fossil Algae*, Berlin: Springer
644 Heidelberg, 248-260.
645 Scholle PA. 1978. *A color illustrated guide to carbonate rock constituents, textures, cements,*
646 *and porosities*. The American Association of Petroleum Geologists, 241pp.
647 Schubert JK, Bottjer DJ. 1992. Early Triassic stromatolites as post-extinction disaster forms.
648 Geology, 20: 883–86.
649 Shapiro RS, Awramik SM. 2000. Microbialite morphostratigraphy as a tool for correlating Late
650 Cambrian–Early Ordovician sequences. The Journal of Geology, 108(2): 171-180.
651 Soria JM, Alfaro P, Fernandez J, Viseras C. 2001. Quantitative subsidence-uplift analysis of the
652 Bajo Segura Basin (eastern Betic Cordillera, Spain): Tectonic control of the stratigraphic
653 architecture. Sedimentary. Geology, 140(3-4): 271-289.
654 Soria JM, Caracuel JE, Yebenes A, Fernandez J, Viseras C. 2005. The stratigraphic record of the
655 Messinian salinity crisis in the northern margin of the Bajo Segura Basin (SE Spain).
656 Sedimentary Geology, 179: 225-247.
657 Soria JM, Caracuel JE, Corbí H, Dinares-Turell J, Lancis C, Tent-Manclus JE, Viseras C,
658 Yebenes A. 2008. The Messinian–early Pliocene stratigraphic record in the southern Bajo
659 Segura Basin (Betic Cordillera, Spain). Implications for the Mediterranean salinity crisis.
660 Sedimentary Geology, 203: 267–288.
661 Soria JM, Giannetti A, Monaco P, Corbí H, García-Ramos D, Viseras C. 2014. Cyclically-
662 arranged, storm-controlled, prograding lithosomes in Messinian terrigenous shelves (Bajo
663 Segura Basin, western Mediterranean). Sedimentary Geology, 310, 1-15.
664 Suosaari EP, Reid RP, Playford PE, Foster JS, Stolz JF, Casaburi G, Eberli GP. 2016. New
665 multi-scale perspectives on the stromatolites of Shark Bay, Western Australia. Scientific
666 reports, 6: 57-70.
667 Suarez Gonzalez P, Quijada IE, Benito MI, Mas R, Merinero R, Riding RE. 2014. Origin and
668 significance of lamination in Lower Cretaceous stromatolites and proposal for a quantitative
669 approach. Sedimentary Geology, 300: 11-27.
670 Tent-Manclus JE. 2003. La estructura y estratigrafia de las sierras de Crevillente, Abanilla y
671 Algayat: su relacion con la falla de Crevillente. D. Phil. Thesis, Universidad de Alicante.
672 Viseras C, Soria JM, Fernandez J. 2004. Cuencas neogenas postorogénicas de la Cordillera
673 Betica. Geologia de Espana, 576-581.
674 Young RB. 1935. A comparison of certain stromatolitic rocks in the Dolomite series of South
675 Africa with marine algal sediments in the Bahamas. Geological Society of South Africa, 37(3-
676 6): 153-162.

677
678

Figure 1

Geological context of the studied section (modified from Gamonal et al., 2018).

(A) Location of the studied basin in the context of the western Mediterranean. (B) Synthetic geological map of the SE Spain in which it is located the Bajo Segura basin. (C) Geological map of the northern sector of the Bajo Segura, where the location of the section is indicated.

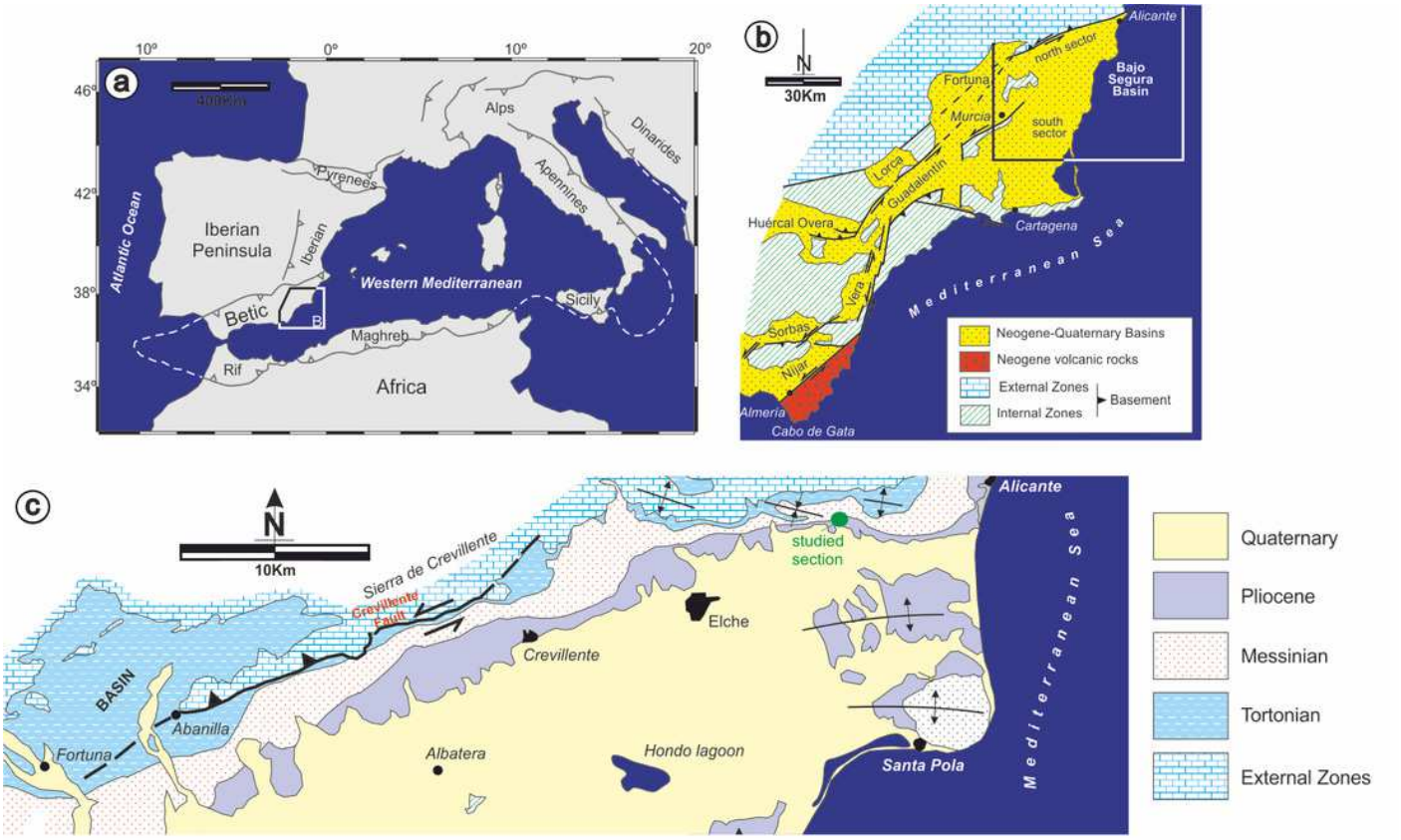

Figure 2

Stratigraphic column for the CAM sequence.

(A) Detail of the stromatolitic level and the end-Messinian discontinuity. (B) Alternation of calcarenite strata in the basal sector of the sequence. (C) Panoramic view of the CAM sequence.

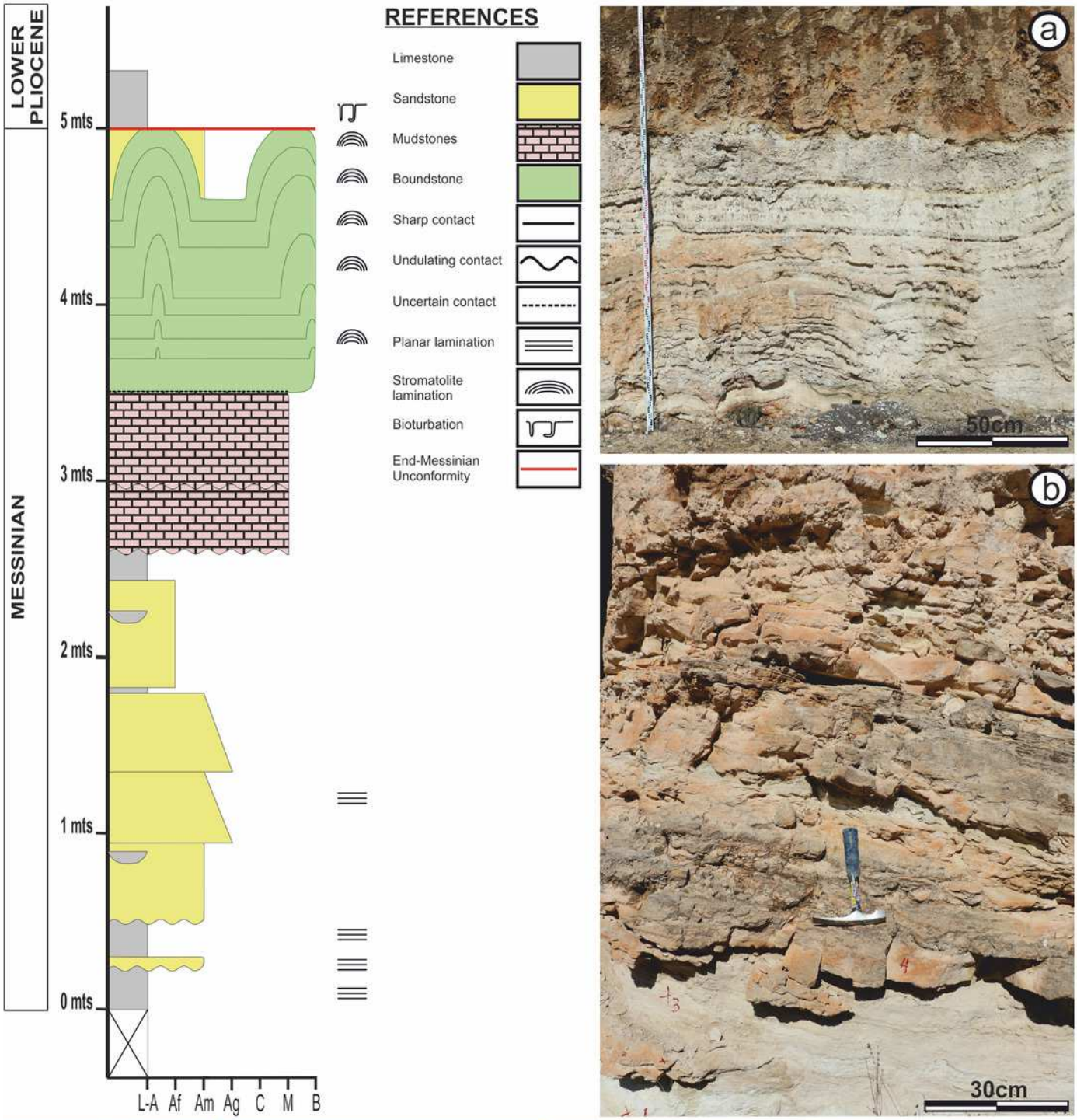

PeerJ Preprints | https://doi.org/10.7287/peerj.preprints.26648v1 | CC BY 4.0 Open Access | rec: 9 Mar 2018, publ: 9 Mar 2018

Figure 3

Architecture and external morphology of the Stromatolites

Image worked on a panoramic photograph of the outcrop, which shows the lateral variation in the morphology and architecture of the stromatolites, together with the relationship of these facies with both the substrate on which they developed as well as with the end-Messinian discontinuity.

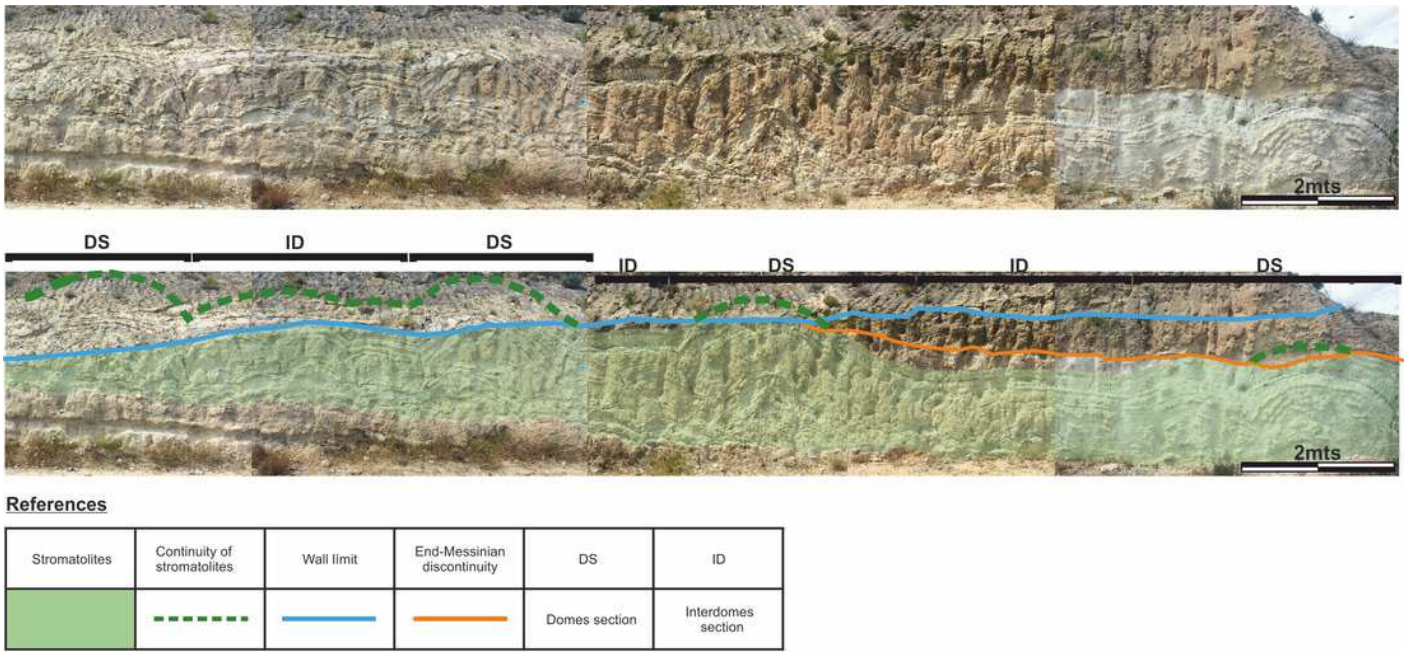

Figure 4

Internal stromatolite morphology: characterization of subfacies.

(A) Photograph of the stromatolitic macrostructure in which the seven subfacies that compose it are indicated (numbered from 1 to 7) and their continuity throughout their horizontal development. (B) View of subfacies 1 in the outcrop. (C) View of subfacies 2 in the outcrop, the lamination (L) by which these subfacies are composed and the porosity present. (D) View of subfacies 3 in the outcrop. The thickness of these subfacies is marked with the dotted line. (E) View of subfacies 4 in the outcrop where it is shown the lamination (L) that composes it. (F) View in which the subfacies 5 are shown in the outcrop, and the lamination (L) that composes it. (G) View showing the subfacies 6 in the outcrop, the columnar structures (C) that compose it and the hiatuses in the lamination (L). (H) View in which the subfacies 7 are shown in the outcrop and the columnar structures (C) that compose it.

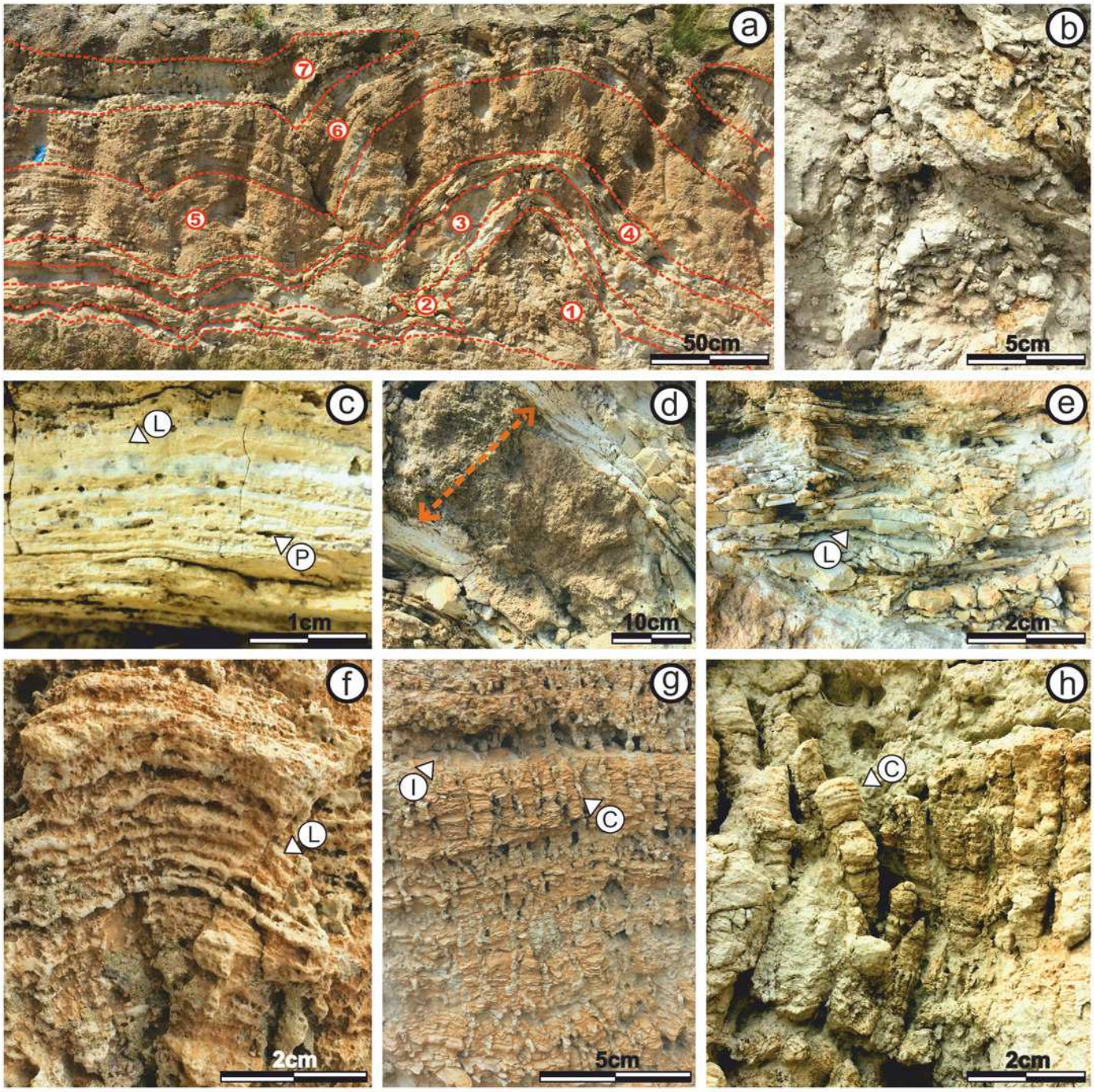

Figure 5

Thin laminae of stromatolitic subfacies 1, 2 and 3.

(A) Subfacies 1 in the interdome sector showing micritic mud of massive texture with no specific geometry or pattern of arrangement, with vuggy type porosity (P). (B) Dome sector in subfacies 1 showing repetitive lamination with 35º slope. (C) Subfacies 2 in the interdome sector showing alternating micritic and intramicritic laminae. (D) Dome sector in subfacies 2 showing alternation of fine, dark, highly wavy micritic laminae. (E) Presence of intraclasts (I) submerged in the micritic matrix in subfacies 3. (F) Oolith (O) submerged in the micritic matrix in subfacies 3.

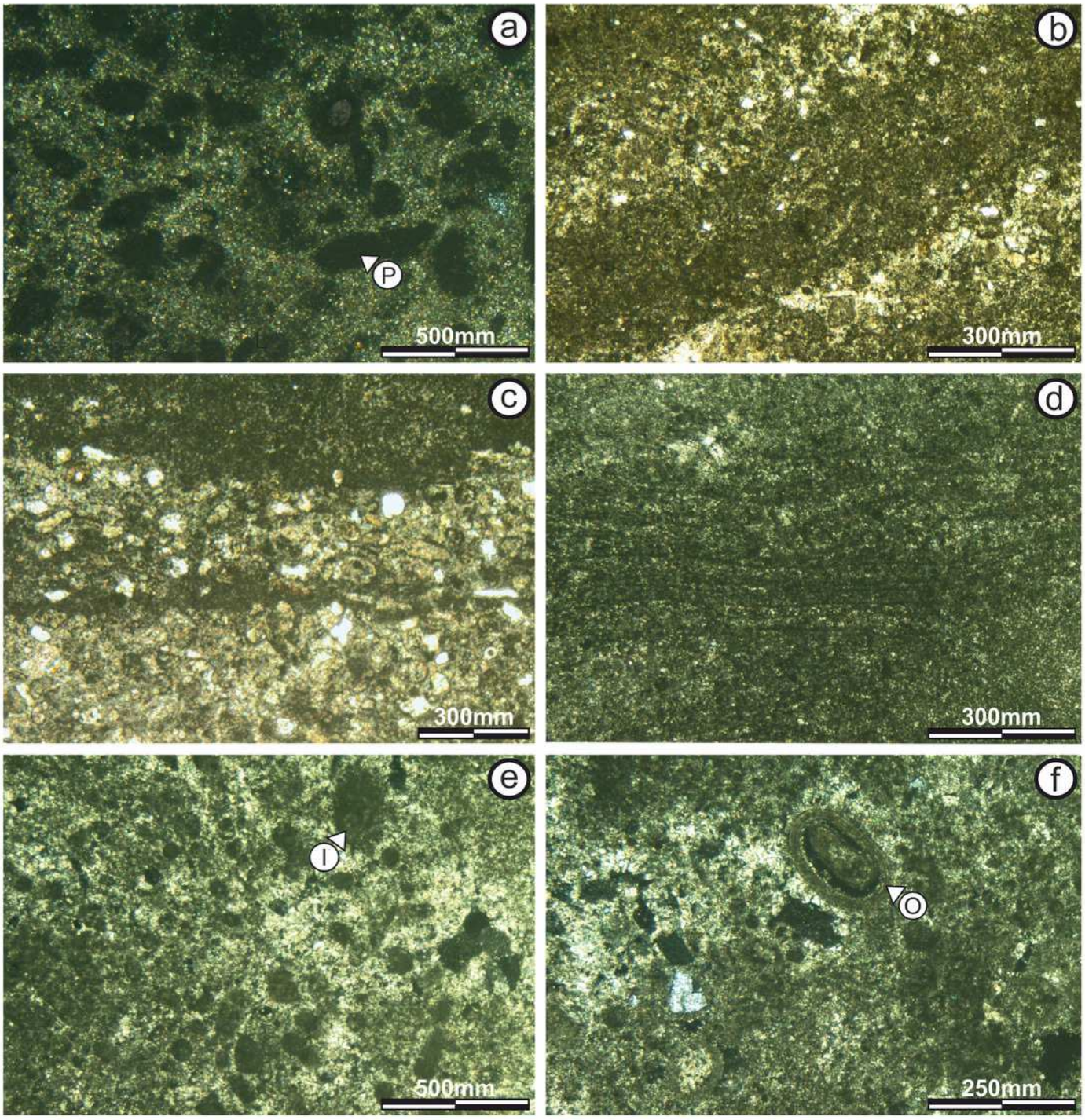

PeerJ Preprints | https://doi.org/10.7287/peerj.preprints.26648v1 | CC BY 4.0 Open Access | rec: 9 Mar 2018, publ: 9 Mar 2018

Figure 6

Thin laminae of stromatolitic subfacies 4 and 5.

(A) Fine micritical film with lateral continuity belonging to the interdomes sector of subfacies 4. (B) Dome sector in subfacies 4 showing repetitive lamination of micritic composition. (C) Alternation of continuous and sinuous micritic sheets of the interdomes sector of the subfacies 5. (D) Sector of domes of subfacies 5 where the alternation of micritic sheets with continuous and sinuous intramicritic sheets is observed.

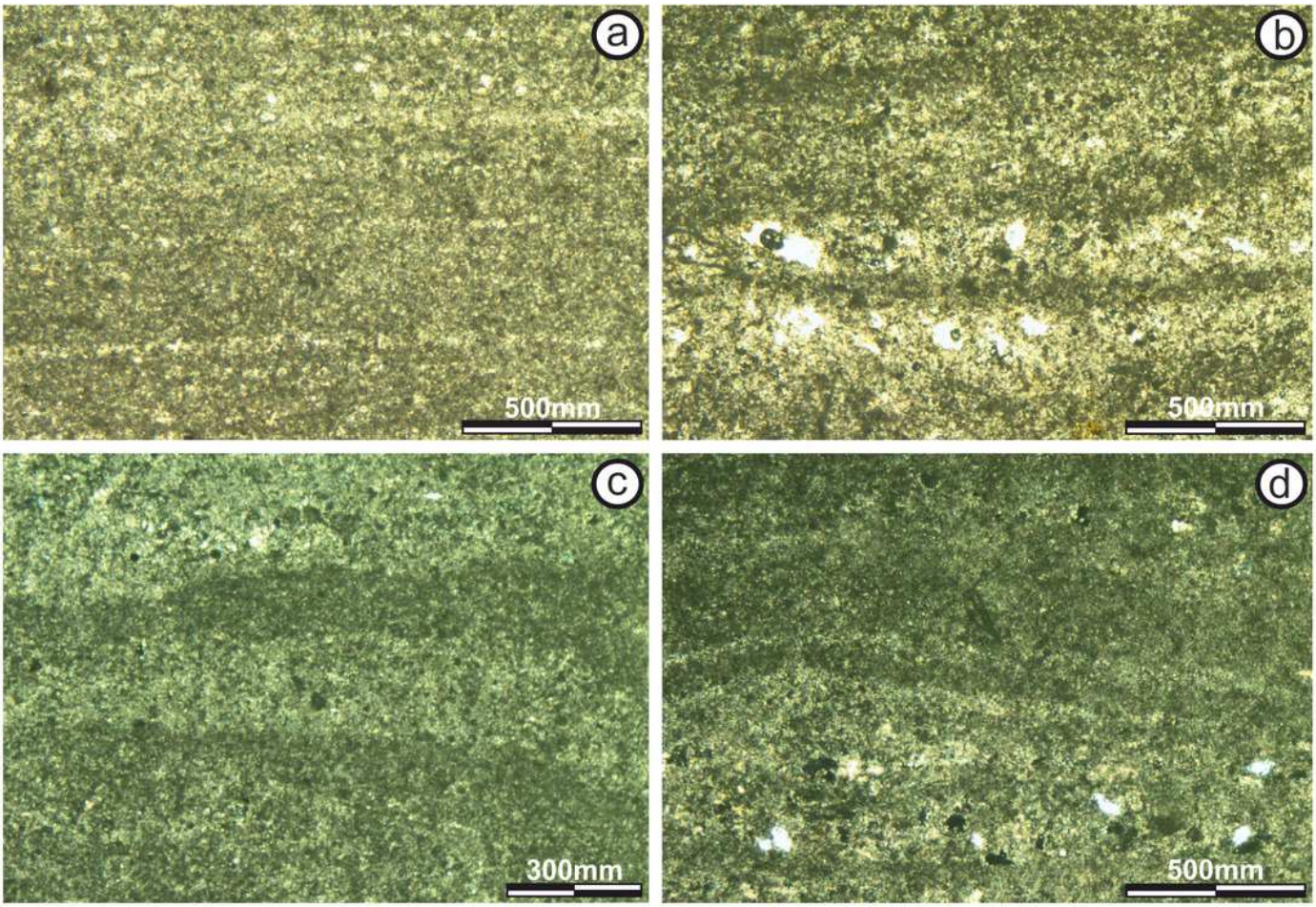

Figure 7

Thin laminae of stromatolitic subfacies 6 and 7.

(A) Fine micritical film with lateral continuity belonging to the interdomes sector of subfacies 6. (B) Photograph corresponding to subfacies 6 in the sector of domes where an alternation is presented of micritic sheets with diffuse edges and concave upward morphology, which are forming the columnar structures. (C) Alternating continuous and sinuous micritic sheets of the interdomes sector of subfacies 7. (D) Possible bioperforation observed in subfacies 7.

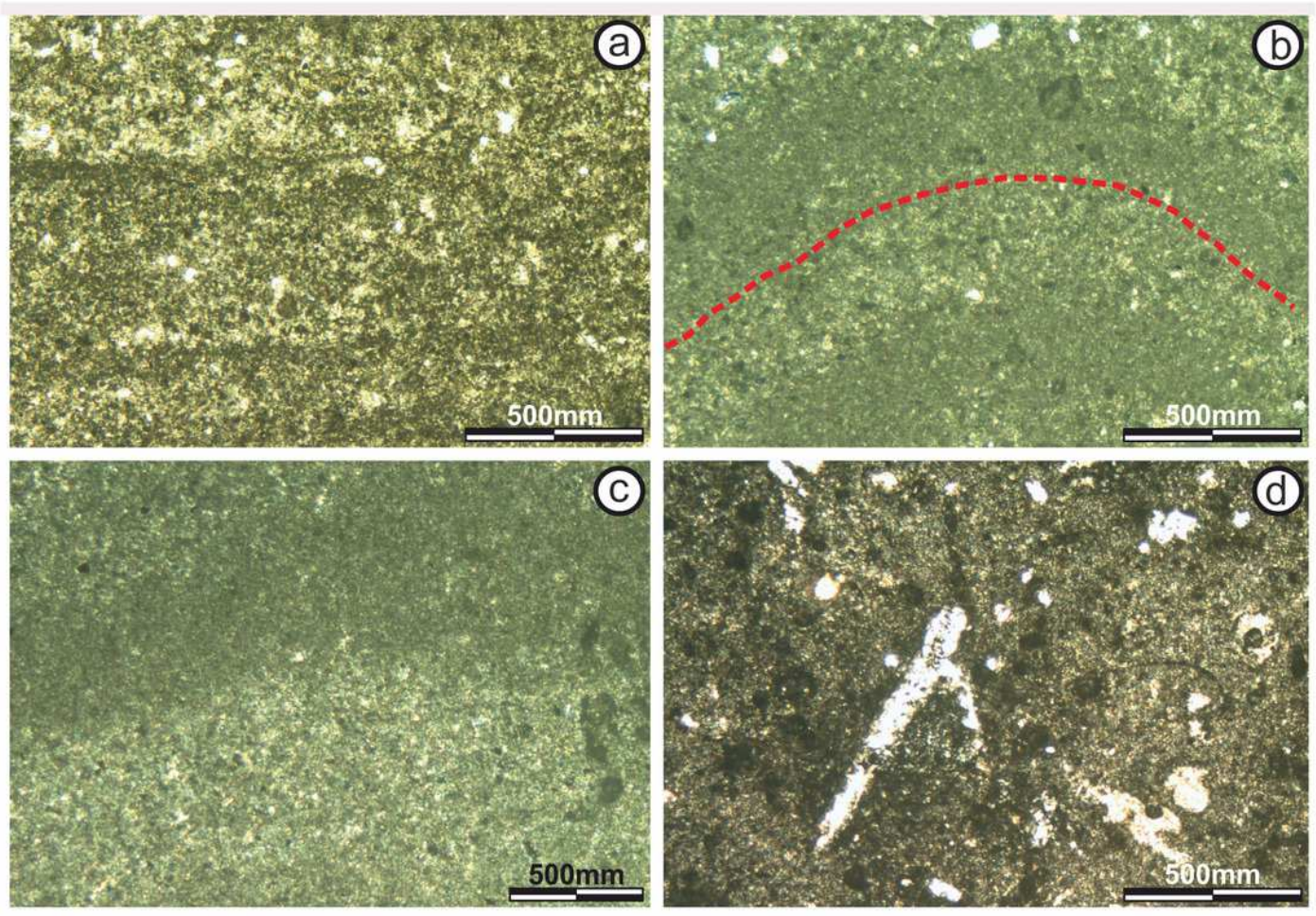

Figure 8

Evolution of the stromatolitic macrostructure over time.

Graph showing the evolution of the stromatolitic macrostructure over time. In it, the seven subfacies are distinguished which are composing the stromatolite, conditioned by the depth and energy of the water.